Acta Mechanica Sinica (2012) 28(5):1479–1487
DOI 10.1007/s10409-012-0148-x

RESEARCH PAPER

Influence of flexible solar arrays on vibration isolation platform of control moment gyroscopes

Yao Zhang · Jing-Rui Zhang · Shi-Jie Xu

Received: 14 January 2012 / Revised: 22 June 2012 / Accepted: 23 August 2012

Abstract A high-performance vibration isolation platform (VIP) has been developed for a cluster of control moment gyroscopes (CMGs). CMGs have long been used for satellite attitude control. In this paper, the influence of flexible solar arrays on a passive multi-strut VIP of CMGs for a satellite is analyzed. The reasonable parameters design of flexible solar arrays is discussed. Firstly, the dynamic model of the integrated satellite with flexible solar arrays, the VIP and CMGs is conducted by Newton–Euler method. Then based on reasonable assumptions, the transmissibility matrix of the VIP is derived. Secondly, the influences of the flexible solar arrays on both the performance of the VIP and the stability of closed-loop control systems are analyzed in detail. The parameter design limitation of these solar arrays is discussed. At last, by selecting reasonable parameters for both the VIP and flexible solar arrays, the attitude stabilization performance with vibration isolation system is predicted via simulation.

Keywords Control moment gyroscope · Vibration isolation platform · Attitude control · Ultra quiet platform

1 Introduction

The control moment gyroscope (CMG) has been used as the actuator of attitude control for modern spacecrafts [1–3]. Because of static and dynamic imbalances of rotor and bearing disturbances, the CMG becomes one of the main vibration sources on spacecrafts. In large complex spacecrafts, the disturbances induced by the CMG can be ignored. However, in some spacecraft having an ultra-precise pointing capability requirement, such as in a space telescope or in a high resolution remote sensing satellite, it is necessary to reduce the vibration caused by the CMG.

Generally, control moment gyroscopes (CMGs) employed are of some kind of configuration, and it is common to use one multi-degree-of-freedom vibration isolation platform (VIP) to interface the cluster of CMGs with the satellite bus [4–6]. Some optical imaging satellites have already used this method to isolate the disturbances caused by CMGs, such as Worldview I, Worldview II and Pleiades-HR [7].

During the past decades, many researchers focused on how to improve the performance of vibration isolator element and have designed some vibration isolators: D-Strut, D-Strut™ 1.5 Hz D-Strut, Adaptable D-Strut™, and Hybrid D-Strut for instance [8–12]. The D-strut manufactured by the Honeywell Inc. is widely used as the vibration isolator element for a VIP. Its effectiveness was sufficiently proved in isolating the vibration of fly wheel on Hubble Space Telescope (HST) [13]. There are abundant researches about the vibration isolation system using these vibration isolator elements. Davis and Wilson [14] tested the efficiency of vibration isolator in HST by doing hardware simulation on earth. Pendergast and Schauwecker [15] designed a passive vibration isolation system for reaction wheel to meet the imaging performance requirement of advance X-ray astrophysics facility (AXAF). This isolation system aligned in a geometry commonly known as a Stewart platform arrangement can reduce multi-dimensional disturbances. Bronowiki [16] gave a detailed description of the vibration isolation system of the James Webb Space Telescope (JWST). The jitter performance using the vibration isolation system of spacecraft was predicted in some missions, such as The Space Interferometer Mission (SIM) [17], The Terrestrial Planet Finder Coronagraph (TPF-C) [18, 19], The GONES-N spacecraft [20] and the Solar Dynamics Observatory (SDO) [21]. In these references, the structures of spacecraft were all modeled using finite element method, where some used the vibration

Y. Zhang (✉) · J.-R. Zhang
School of Aerospace Engineering,
Beijing Institute of Technology, 100081 Beijing, China
e-mail: zhangyao7000@yahoo.cn
S.-J. Xu
School of Astronautics,
Beihang University, 100191 Beijing, China

isolation system consisting of 6 decoupled 2nd-order low-pass filters to approximate the effect of a passive fly wheel mount [22, 23]. These accurate finite element models are necessary to predict the jitter performance of the spacecraft. However, the analysis method using finite element models has some limitations: The spacecraft structure should be well known, the dynamic coupling can not be obtained, and the finite element model is not suitable for attitude controller design based on modern control theory for instance.

In previous work, an integrated satellite dynamic model including the VIP and pyramid configuration CMGs was built. The influence of the vibration isolation system on the attitude control system of the satellite was also analyzed in detail [24]. However, the dynamic model of the satellite ignores the flexible solar arrays. Actually, some studies show that these flexible solar arrays do affect the vibration isolation platform characteristics and the attitude control system stability [25, 26]. Therefore, in order to manufacture a satisfactory VIP of CMGs, it is necessary to analyze the influence of flexible solar arrays on both the VIP system and the stability of attitude control system.

In this paper, the performance of a passive multi-strut VIP of CMGs is discussed for a satellite with flexible solar arrays. An integrated satellite dynamic model including the VIP, pyramid configuration CMGs and the flexible solar arrays is built. Then the transmissibility matrix of the VIP with two-parameter isolators is obtained. The influence of the flexible solar arrays on the performance of the vibration isolation platform and on the stability of the attitude control system is analyzed in detail.

2 Dynamic model of the integrated satellite

In this study, CMGs are in pyramid configuration and the mass of each CMG is 19 kg. The passive multi-strut VIP is a Stewart platform with cubic configuration and has 6 extensible struts [27, 28]. Each strut of the platform includes an upper part, a lower part and spring and damper to connect the two parts. The legs are connected to the upper platform by spherical joints, and to the base platform by universal joints. Figure 1 gives a schematic representation of the satellite.

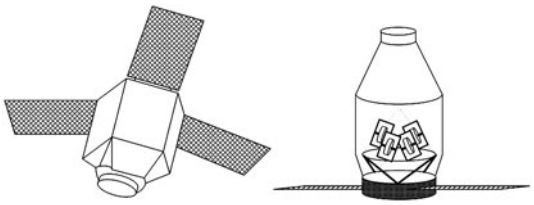

Fig. 1 The satellite configuration

Because CMGs are fixed at the upper platform, CMGs and the upper platform are taken as the upper platform system, while the satellite with flexible solar arrays and the base platform are taken as the base platform system. The kinematic and dynamic models of each strut are firstly derived. Then based on the forces and torques which are given respectively for the upper and the base platform systems, the dynamic models of these two systems are established. According to the kinematic and dynamic models of the base platform system, the attitude information of the satellite can be obtained.

In addition, there are no control forces acting on the flexible solar arrays in engineering. Because the angular velocities of the central rigid body, the angular velocities and the elastic vibration velocities of the flexible solar arrays with respect to the central rigid body are small, and high order nonlinear coupling terms caused by the multiplication of above velocities are negligible. Based on the above assumptions and the structural property of the satellite, dynamic equations can be obtained for the upper and the base platform systems, respectively.

The coordinate frames of the satellite system are shown in Fig. 2, in which f_u is the upper platform system frame, f_d is the base platform frame, f_b is the satellite body frame, $f_{\mathrm{f}j}$ is the j-th flexible solar array frame, A_{mn} represents the transformation matrix from f_n to f_m which can be any two frames.

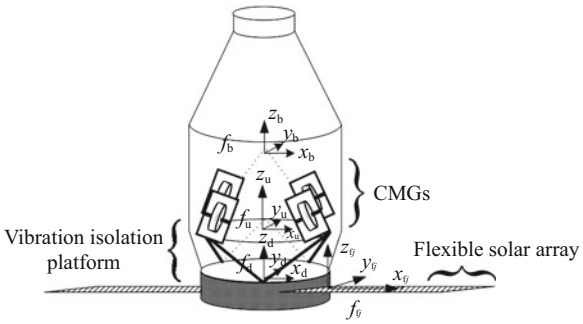

Fig. 2 Coordinate frames of the satellite system

The dynamic equations of the upper platform system can be described as

$$
\begin{aligned}
&m_\mathrm{p}\dot{\boldsymbol{v}}_\mathrm{p} - \boldsymbol{S}_\mathrm{p}^{\times}\dot{\boldsymbol{\omega}}_\mathrm{p} = -\boldsymbol{A}_\mathrm{ue}\sum_{i=1}^{N}\boldsymbol{F}_{si} + \boldsymbol{F}_\mathrm{d},\\
&\boldsymbol{I}_\mathrm{p}\dot{\boldsymbol{\omega}}_\mathrm{p} + \boldsymbol{\omega}_\mathrm{p}^{\times}\boldsymbol{I}_\mathrm{p}\boldsymbol{\omega}_\mathrm{p} + \boldsymbol{S}_\mathrm{p}^{\times}\dot{\boldsymbol{v}}_\mathrm{p}\\
&\qquad = \boldsymbol{T}_\mathrm{c} - \sum_{i=1}^{N}\boldsymbol{p}_i^{\times}\boldsymbol{A}_\mathrm{ue}\boldsymbol{F}_{si} + \sum_{i=1}^{N}\boldsymbol{F}_{\mathrm{p}i} + \boldsymbol{T}_\mathrm{d},
\end{aligned}
\tag{1}
$$

where the variables with index i represent the i-th leg variables, which means that the equations are applicable to any leg in general. N is the number of struts; m_p is the mass of upper platform system; $\boldsymbol{I}_\mathrm{p}$ is the moment of inertia of upper platform system; $\boldsymbol{S}_\mathrm{p}$ is the static moment of upper platform system; "$\times$" denotes the skew-symmetric matrix for vector cross product; $\boldsymbol{v}_\mathrm{p}$ represents the absolute velocity of point o_u; $\boldsymbol{\omega}_\mathrm{p}$ is the angular velocity of the upper platform system; $\boldsymbol{p}_i$ is the vector from the mass center of the upper platform to the upper platform connection point as shown in Fig. 3; $\boldsymbol{F}_{si}$

is the constraint force at the spherical joint acting on upper part; $\boldsymbol{T}_{\mathrm{c}}$ is the output torque provided by CMGs; $\boldsymbol{F}_{\mathrm{d}}$ and $\boldsymbol{T}_{\mathrm{d}}$ are respectively the disturbances force and torque caused by CMGs; $\boldsymbol{F}_{\mathrm{p}i} = c_{si}(\boldsymbol{A}_{\mathrm{ue}}\boldsymbol{\omega}_{\mathrm{l}i} - \boldsymbol{\omega}_{\mathrm{p}})$ is the moment of viscous friction at spherical joint; c_{si} is the coefficient of viscous friction in the spherical; $\boldsymbol{\omega}_{\mathrm{l}i}$ is the angular velocity of each strut; $\boldsymbol{A}_{\mathrm{ue}}$ is the transformation matrix from the inertial frame to upper platform system frame.

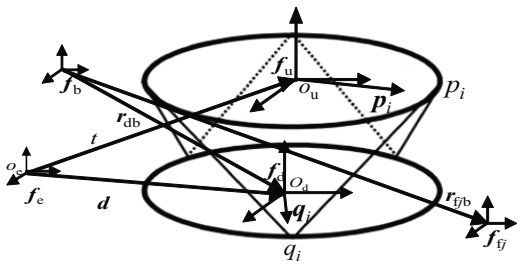

Fig. 3 Coordinate frame of the vibration isolation platform

Taking into account these flexible solar arrays, one can express the attitude dynamics of the base platform system by the following equations

$$
\begin{aligned}
&m_{\mathrm{b}}\dot{\boldsymbol{v}}_{\mathrm{b}} - \boldsymbol{S}_{\mathrm{b}}^{\times}\dot{\boldsymbol{\omega}}_{\mathrm{b}} + \sum_{j=1}^{3}\boldsymbol{A}_{\mathrm{f}j\mathrm{b}}^{\mathrm{T}}\boldsymbol{S}_{\mathrm{f}j}^{\mathrm{T}}\dot{\boldsymbol{\omega}}_{\mathrm{f}j} + \sum_{j=1}^{3}\boldsymbol{A}_{\mathrm{f}j\mathrm{b}}^{\mathrm{T}}\boldsymbol{P}_{\mathrm{f}j}\ddot{\boldsymbol{q}}_{\mathrm{f}j} = \\
&\quad -\boldsymbol{A}_{\mathrm{be}}\sum_{i=1}^{N}\boldsymbol{F}_{\mathrm{u}i} + \boldsymbol{F}_{\mathrm{ext}}, \\
&\boldsymbol{I}_{\mathrm{b}}\dot{\boldsymbol{\omega}}_{\mathrm{b}} + \boldsymbol{\omega}_{\mathrm{b}}^{\times}\boldsymbol{I}_{\mathrm{b}}\boldsymbol{\omega}_{\mathrm{b}} + \boldsymbol{S}_{\mathrm{b}}^{\times}\dot{\boldsymbol{v}}_{\mathrm{b}} + \sum_{j=1}^{3}(\boldsymbol{r}_{\mathrm{bf}j}^{\times}\boldsymbol{A}_{\mathrm{f}j\mathrm{b}}^{\mathrm{T}}\boldsymbol{S}_{\mathrm{f}j}^{\times} + \boldsymbol{A}_{\mathrm{f}j\mathrm{b}}^{\mathrm{T}}\boldsymbol{I}_{\mathrm{f}j})\dot{\boldsymbol{\omega}}_{\mathrm{f}j} \\
&\quad + \sum_{j=1}^{3}(\boldsymbol{A}_{\mathrm{f}j\mathrm{b}}^{\mathrm{T}}\boldsymbol{H}_{\mathrm{f}j} + r_{\mathrm{bf}j}^{\times}\boldsymbol{A}_{\mathrm{f}j\mathrm{b}}^{\mathrm{T}}\boldsymbol{P}_{\mathrm{f}j})\ddot{\boldsymbol{q}}_{\mathrm{f}j} \\
&\quad = -\sum_{i=1}^{N}(\boldsymbol{A}_{\mathrm{bd}}\boldsymbol{q}_i + \boldsymbol{r}_{\mathrm{db}})^{\times}(\boldsymbol{A}_{\mathrm{be}}\boldsymbol{F}_{\mathrm{u}i}) \\
&\quad + \sum_{i=1}^{N}\boldsymbol{F}_{\mathrm{q}i} + \boldsymbol{M}_{\mathrm{ext}} - \boldsymbol{A}_{\mathrm{be}}\sum_{i=1}^{N}\boldsymbol{M}_{\mathrm{u}i}\boldsymbol{h}_{\mathrm{u}i}.
\end{aligned}
\tag{2}
$$

The rotation equation of the j-th flexible solar arrays can be described as

$$
\begin{aligned}
&\boldsymbol{I}_{\mathrm{f}j}\dot{\boldsymbol{\omega}}_{\mathrm{f}j} + \boldsymbol{H}_{\mathrm{f}j}\ddot{\boldsymbol{q}}_{\mathrm{f}j} + (-\boldsymbol{S}_{\mathrm{f}j}^{\times}\boldsymbol{A}_{\mathrm{f}j\mathrm{b}}r_{\mathrm{bf}j}^{\times} + \boldsymbol{I}_{\mathrm{f}j}\boldsymbol{A}_{\mathrm{f}j\mathrm{b}})\dot{\boldsymbol{\omega}}_{\mathrm{b}} + \boldsymbol{S}_{\mathrm{f}j}^{\times}\boldsymbol{A}_{\mathrm{f}j\mathrm{b}}\dot{\boldsymbol{v}}_{\mathrm{b}} \\
&\quad = \boldsymbol{T}_{\mathrm{f}j}.
\end{aligned}
\tag{3}
$$

The vibration equation of the j-th flexible solar array can be described as

$$
\begin{aligned}
&\boldsymbol{M}_{\mathrm{f}j}\ddot{\boldsymbol{q}}_{\mathrm{f}j} + \boldsymbol{P}_{\mathrm{f}j}^{\mathrm{T}}\boldsymbol{A}_{\mathrm{f}j\mathrm{b}}\dot{\boldsymbol{v}}_{\mathrm{b}} + (-\boldsymbol{P}_{\mathrm{f}j}^{\mathrm{T}}\boldsymbol{A}_{\mathrm{f}j\mathrm{b}}\boldsymbol{r}_{\mathrm{bf}j}^{\times} + \boldsymbol{H}_{\mathrm{f}j}^{\mathrm{T}}\boldsymbol{A}_{\mathrm{f}j\mathrm{b}})\dot{\boldsymbol{\omega}}_{\mathrm{b}} \\
&\quad + \boldsymbol{H}_{\mathrm{f}j}^{\mathrm{T}}\dot{\boldsymbol{\omega}}_{\mathrm{f}j} + \boldsymbol{C}_{\mathrm{f}j}\dot{\boldsymbol{q}}_{\mathrm{f}j} + \boldsymbol{K}_{\mathrm{f}j}\boldsymbol{q}_{\mathrm{f}j} = \boldsymbol{0},
\end{aligned}
\tag{4}
$$

where m_{b} and $\boldsymbol{I}_{\mathrm{b}}$ are the mass and the moment of inertia of base platform system, respectively, $\boldsymbol{M}_{\mathrm{f}j}$ is the model mass of the j-th flexible array, $\boldsymbol{I}_{\mathrm{f}j}$ is the moment of inertia of the j-th flexible array, $\boldsymbol{v}_{\mathrm{b}}$ represents the absolute velocity of point o_{b}, $\boldsymbol{\omega}_{\mathrm{b}}$ is the angular velocity of base platform system, $\boldsymbol{\omega}_{\mathrm{f}j}$ is the angular velocities of the j-th flexible solar array with respect to the central rigid body, $\boldsymbol{q}_{\mathrm{f}j}$ is the first m orders modal coordinates of the j-th flexible solar array, $\boldsymbol{S}_{\mathrm{b}}$ is the static moment of base platform system, $\boldsymbol{S}_{\mathrm{f}j}$ is the static moment of the j-th flexible solar array, $\boldsymbol{P}_{\mathrm{f}j}$ is modal momentum matrix of the j-th flexible solar array, $\boldsymbol{H}_{\mathrm{f}j}$ is modal angular momentum matrix of the j-th flexible solar array, $\boldsymbol{C}_{\mathrm{f}j}$ and $\boldsymbol{K}_{\mathrm{f}j}$ are the modal damping and modal stiffness of the j-th flexible solar array, respectively, $\boldsymbol{A}_{\mathrm{bd}}$ is the transformation matrix from the base platform frame to the satellite body frame, $\boldsymbol{A}_{\mathrm{f}j\mathrm{b}}$ is the transformation matrix from the satellite body frame to the j-th flexible solar array, $\boldsymbol{r}_{\mathrm{db}}$ is the vector from the centre of satellite body frame to the centre of base platform frame as shown in Fig. 3, $\boldsymbol{q}_i$ is the vector from the mass center of base platform to the i-th base platform connection point as shown in Fig. 3, $\boldsymbol{r}_{\mathrm{bf}j}$ is the vector from the centre of satellite body frame to the centre of the j-th flexible solar array frame, $\boldsymbol{F}_{\mathrm{u}i}$ is the constraint force at the universal joint acting on lower part, $\boldsymbol{M}_{\mathrm{u}i}$ is the magnitude of the constraint moment at the universal joint acting about strut axis, $c_{\mathrm{u}i}$ is the coefficient of viscous friction in universal joints, $\boldsymbol{F}_{\mathrm{ext}}$ and $\boldsymbol{T}_{\mathrm{ext}}$ are the external disturbing force and torque acting on the satellite respectively, $\boldsymbol{T}_{\mathrm{f}j}$ is the torque acting on the j-th flexible solar array, $\boldsymbol{F}_{\mathrm{q}i} = c_{\mathrm{u}i}(\boldsymbol{A}_{\mathrm{be}}\boldsymbol{\omega}_{\mathrm{l}i} - \boldsymbol{\omega}_{\mathrm{b}})$ is the moment of viscous friction at universal joint, $\boldsymbol{A}_{\mathrm{be}}$ is the transformation matrix from the inertial frame to the satellite body frame.

The expressions of $\boldsymbol{F}_{si}$ and $\boldsymbol{F}_{\mathrm{u}i}$ have been derived by Zhang and Xu [29], so in this paper they are not given in detail.

The present study focuses on the disturbances of CMG caused by the static and dynamic imbalance of rotor, the non-verticality and non-crossing between gimbal axis and rotor axis as well as the deviation of mass centre of the CMG system from the gimbal rotation axis etc. According to the analyses of previous studies [30], we knew that the installation error and the coupling disturbance terms are negligible. Then the simplified dynamic equations of disturbances of CMGs are as follows for the upper platform system frame.

$$
\boldsymbol{F}_{\mathrm{d}} = \sum_{h=1}^{M}\left(-m_{\mathrm{w}h}\boldsymbol{A}_{\mathrm{uw}h}\boldsymbol{\Omega}_h^{\times}\boldsymbol{\Omega}_h^{\times}\boldsymbol{\rho}_{\mathrm{w}h}\right) \tag{5}
$$

$$
\begin{aligned}
\boldsymbol{T}_{\mathrm{d}} = &\sum_{h=1}^{M}\{\boldsymbol{r}_{\mathrm{fu}h}^{\times}(-m_{\mathrm{w}h}\boldsymbol{A}_{\mathrm{uw}h}\boldsymbol{\Omega}_h^{\times}\boldsymbol{\Omega}_h^{\times}\boldsymbol{\rho}_{\mathrm{w}h}) \\
&+ \boldsymbol{A}_{\mathrm{uw}h}[\boldsymbol{I}_{\mathrm{ww}h}^{o_{\mathrm{f}}}\boldsymbol{\Omega}_h^{\times} + (\boldsymbol{I}_{\mathrm{ww}h}^{o_{\mathrm{f}}}\boldsymbol{\Omega}_h^{\times})^{\mathrm{T}}]\boldsymbol{\Omega}_h\}
\end{aligned}
\tag{6}
$$

where, the variables with index h represent the h-th CMG variables, which means that the equations are applicable to any CMG in general. M is the number of CMG; $m_{\mathrm{w}h}$ is the mass of the h-th rotor; h means the h-th CMG. $\boldsymbol{A}_{\mathrm{uw}h}$ is the transformation matrix from the geometric body frame of the h-th rotor to the upper platform system frame; $\boldsymbol{\Omega}_h$ represents the angular velocity of the h-th rotor with respect to the upper platform system; $\boldsymbol{\rho}_{\mathrm{w}h}$ represents the offset of center of mass

of the h-th rotor from its spin axis; $\boldsymbol{r}_{\mathrm{fu}h}$ is the vector from the centre of upper platform system frame to the geometric centre of the h-th rotor; $\boldsymbol{I}^{o_{\mathrm{f}}}_{\mathrm{ww}h} = \boldsymbol{A}_{\mathrm{wl}h}\boldsymbol{I}^{o_{\mathrm{l}}}_{\mathrm{wl}h}\boldsymbol{A}_{\mathrm{lw}h} + m_{\mathrm{w}h}(\boldsymbol{\rho}^{\mathrm{T}}_{\mathrm{w}h}\boldsymbol{\rho}_{\mathrm{w}h}E_3 - \boldsymbol{\rho}_{\mathrm{w}h}\boldsymbol{\rho}^{\mathrm{T}}_{\mathrm{w}h})$, is the moment of inertia of the h-th rotor with respect to its geometric centre in the geometric body frame of the rotor; $\boldsymbol{I}^{o_{\mathrm{l}}}_{\mathrm{wl}h} = \mathrm{diag}(\ I_{\mathrm{wl}x}\ \ I_{\mathrm{wl}y}\ \ I_{\mathrm{wl}z}\ )$, is the moment of inertia of rotor with respect to its centroid; E_3 is the 3×3 identity matrix; $\boldsymbol{A}_{\mathrm{wl}h}$ is the dynamic imbalance of the h-th rotor which is caused by the misalignment of rotor's principle axis and rotation axis.

Thus, the integrated satellite dynamic model is the combination of Eqs. (1)–(6).

3 Frequency domain characteristics of the VIP

In this section, the dynamic model of the integrated satellite is firstly simplified according to some reasonable assumptions. Then the transmissibility matrix of the vibration isolation system is obtained. At last, the influences of the flexible solar arrays on both the performance of the VIP and the stability of closed-loop control system are analyzed in detail by frequency-domain analysis method.

3.1 Transmissibility matrix of the VIP

To analyze the frequency domain characteristics of the VIP and the influence of flexible solar arrays on satellite systems, the following assumptions are made:

Assumption 1 The platform configuration does not change because the amplitude of vibration is small. The transformation matrix $\boldsymbol{A}_{\mathrm{bd}}$ from the satellite body frame to the base platform frame is an identity matrix according to the position relation between the satellite and the VIP.

Assumption 2 The transformation matrixes $\boldsymbol{A}_{\mathrm{eu}}$ and $\boldsymbol{A}_{\mathrm{eb}}$ which are respectively from the upper and base platform frames to the inertial frame can be seen as identity matrixes, and the square of angular velocities can be ignored because both the attitude angles and the angular velocities are small under attitude stabilization control.

Assumption 3 Because the influence of strut's moment of inertia and mass on the transfer function of the VIP is small, they can be ignored.

Assumption 4 The angular velocities of flexible solar arrays with respect to the central rigid body can be seen as zero, because the flexible solar arrays considered is in a locked state as shown by Fig. 1.

Based on the above assumptions, the simplified dynamic equations of the integrated satellite are given as

$$
\begin{aligned}
&m_{\mathrm{p}}\ddot{\boldsymbol{t}} - \boldsymbol{S}^{\times}_{\mathrm{p}}\ddot{\boldsymbol{\theta}}_{\mathrm{p}} = -\sum_{i=1}^{N}\boldsymbol{F}_{\mathrm{s}i} + \boldsymbol{F}_{\mathrm{d}},\\
&\boldsymbol{I}_{\mathrm{p}}\ddot{\boldsymbol{\theta}}_{\mathrm{p}} + \boldsymbol{S}^{\times}_{\mathrm{p}}\ddot{\boldsymbol{t}} = -\sum_{i=1}^{N}\boldsymbol{p}_i^{\times}\boldsymbol{F}_{\mathrm{s}i} + \boldsymbol{T}_{\mathrm{d}},
\end{aligned}
\tag{7}
$$

$$
\begin{aligned}
&m_{\mathrm{b}}\ddot{\boldsymbol{b}} - \boldsymbol{S}^{\times}_{\mathrm{b}}\ddot{\boldsymbol{\theta}}_{\mathrm{b}} + \sum_{j=1}^{3}\boldsymbol{A}^{\mathrm{T}}_{\mathrm{f}j\mathrm{b}}\boldsymbol{P}_{\mathrm{f}j}\ddot{\boldsymbol{q}}_{\mathrm{f}j} = -\sum_{i=1}^{N}\boldsymbol{F}_{\mathrm{u}i},\\
&\boldsymbol{I}_{\mathrm{b}}\ddot{\boldsymbol{\theta}}_{\mathrm{b}} + \boldsymbol{S}^{\times}_{\mathrm{b}}\ddot{\boldsymbol{b}} + \sum_{j=1}^{3}\boldsymbol{A}^{\mathrm{T}}_{\mathrm{f}j\mathrm{b}}\boldsymbol{H}_{\mathrm{bf}j}\ddot{\boldsymbol{q}}_{\mathrm{f}j} = -\sum_{i=1}^{N}(\boldsymbol{q}_i + \boldsymbol{r}_{\mathrm{db}})^{\times}\boldsymbol{F}_{\mathrm{u}i},\\
&\boldsymbol{M}_{\mathrm{f}j}\ddot{\boldsymbol{q}}_{\mathrm{f}j} + \boldsymbol{P}^{\mathrm{T}}_{\mathrm{f}j}\boldsymbol{A}_{\mathrm{f}j\mathrm{b}}\ddot{\boldsymbol{b}} + \boldsymbol{H}^{\mathrm{T}}_{\mathrm{bf}j}\boldsymbol{A}_{\mathrm{f}j\mathrm{b}}\ddot{\boldsymbol{\theta}}_b + \boldsymbol{C}_{\mathrm{f}j}\dot{\boldsymbol{q}}_{\mathrm{f}j} + \boldsymbol{K}_{\mathrm{f}j}\boldsymbol{q}_{\mathrm{f}j} = \boldsymbol{0},
\end{aligned}
\tag{8}
$$

where, Eq. (7) is the dynamic equations of the upper platform system, Eq. (8) is the dynamic equations of the base platform system, $\boldsymbol{\theta}_{\mathrm{p}}$ and $\boldsymbol{\theta}_{\mathrm{b}}$ are the attitude angles of upper platform system and satellite, respectively, $\boldsymbol{t}$ is the position vector from the center of inertial frame to the mass center of upper platform, and $\boldsymbol{b}$ is the position vector from the center of inertial frame to the satellite.

For two-parameter isolators, the constraint force at the spherical joint acting on the upper part $\boldsymbol{F}_{\mathrm{s}i}$ can be simply described as

$$
\begin{aligned}
\boldsymbol{F}_{\mathrm{s}i} =\ & k_i\boldsymbol{s}_{\mathrm{u}i}\boldsymbol{s}^{\mathrm{T}}_{\mathrm{u}i}t - k_i\boldsymbol{s}_{\mathrm{u}i}\boldsymbol{s}^{\mathrm{T}}_{\mathrm{u}i}\boldsymbol{p}_i^{\times}\boldsymbol{\theta}_{\mathrm{p}} - k_i\boldsymbol{s}_{\mathrm{u}i}\boldsymbol{s}^{\mathrm{T}}_{\mathrm{u}i}\boldsymbol{b}\\
&+ k_i\boldsymbol{s}_{\mathrm{u}i}\boldsymbol{s}^{\mathrm{T}}_{\mathrm{u}i}(\boldsymbol{q}_i + \boldsymbol{r}_{\mathrm{db}})^{\times}\boldsymbol{\theta}_{\mathrm{b}} + c_i\boldsymbol{s}_{\mathrm{u}i}\boldsymbol{s}^{\mathrm{T}}_{\mathrm{u}i}\dot{\boldsymbol{t}} - c_i\boldsymbol{s}_{\mathrm{u}i}\boldsymbol{s}^{\mathrm{T}}_{\mathrm{u}i}\boldsymbol{p}_i^{\times}\dot{\boldsymbol{\theta}}_{\mathrm{p}}\\
&- c_i\boldsymbol{s}_{\mathrm{u}i}\boldsymbol{s}^{\mathrm{T}}_{\mathrm{u}i}\dot{\boldsymbol{b}} + c_i\boldsymbol{s}_{\mathrm{u}i}\boldsymbol{s}^{\mathrm{T}}_{\mathrm{u}i}(\boldsymbol{q}_i + \boldsymbol{r}_{\mathrm{db}})^{\times}\dot{\boldsymbol{\theta}}_{\mathrm{b}},
\end{aligned}
\tag{9}
$$

where, k_i and c_i are the real parameters of the two-parameter isolator, and k_i is the stiffness coefficient, c_i is the damping coefficient, $\boldsymbol{p}_i$ is the vector from the mass center of upper platform to the upper platform connection point, $\boldsymbol{q}_i$ is the vector from the mass center of base platform to the base platform connection point, and $\boldsymbol{s}_{\mathrm{u}i}$ is the unit vector along the strut.

Denote $\boldsymbol{S} = \boldsymbol{s}_{\mathrm{u}i}\boldsymbol{s}^{\mathrm{T}}_{\mathrm{u}i}$,

$$
\boldsymbol{x} = \left[\ \boldsymbol{t}^{\mathrm{T}}\ \boldsymbol{\theta}^{\mathrm{T}}_{\mathrm{p}}\ \boldsymbol{t}^{\mathrm{T}}_{\mathrm{pl}}\ \boldsymbol{\theta}^{\mathrm{T}}_{\mathrm{pl}}\ \boldsymbol{b}^{\mathrm{T}}\ \boldsymbol{\theta}^{\mathrm{T}}_{\mathrm{b}}\ \boldsymbol{q}^{\mathrm{T}}_{\mathrm{f}1}\ \boldsymbol{q}^{\mathrm{T}}_{\mathrm{f}2}\ \boldsymbol{q}^{\mathrm{T}}_{\mathrm{f}3}\ \right]^{\mathrm{T}},
$$

$$
\boldsymbol{J}_i = \left[\ \boldsymbol{S}\ \ -\boldsymbol{S}\boldsymbol{p}_i^{\times}\ \ -\boldsymbol{S}\ \ \boldsymbol{S}(\boldsymbol{q}_i + \boldsymbol{r}_{\mathrm{db}})^{\times}\ \ \boldsymbol{0}_{3\times 3m}\ \right].
$$

Then Eq. (9) can also be rewritten as

$$
\boldsymbol{F}_{\mathrm{s}i} = k_i\boldsymbol{J}_i\boldsymbol{x} + c_i\boldsymbol{J}_i\dot{\boldsymbol{x}}.
\tag{10}
$$

Equations (7) and (8) can be rewritten as

$$
\boldsymbol{M}\ddot{\boldsymbol{x}} + \boldsymbol{C}\dot{\boldsymbol{x}} + \boldsymbol{K}\boldsymbol{x} = \boldsymbol{U},
\tag{11}
$$

where,

$$
\boldsymbol{M} = \mathrm{diag}\left(\left[\ \boldsymbol{M}_1\ \ \boldsymbol{M}_2\ \right]\right),
$$

$$
\boldsymbol{M}_1 = \begin{bmatrix} m_{\mathrm{p}}\boldsymbol{E}_3 & -\boldsymbol{S}^{\times}_{\mathrm{p}} \\ \boldsymbol{S}^{\times}_{\mathrm{p}} & \boldsymbol{I}_{\mathrm{p}} \end{bmatrix},
$$

$$
\boldsymbol{M}_2 = \begin{bmatrix} m_{\mathrm{b}}\boldsymbol{E}_3 & -\boldsymbol{S}^{\times}_{\mathrm{b}} & \boldsymbol{A}^{\mathrm{T}}_{\mathrm{f}j\mathrm{b}}\boldsymbol{P}_{\mathrm{f}j} \\ \boldsymbol{S}^{\times}_{\mathrm{b}} & \boldsymbol{I}_{\mathrm{b}} & \boldsymbol{A}^{\mathrm{T}}_{\mathrm{f}j\mathrm{b}}\boldsymbol{H}_{\mathrm{bf}j} \\ \boldsymbol{P}^{\mathrm{T}}_{\mathrm{f}j}\boldsymbol{A}_{\mathrm{f}j\mathrm{b}} & \boldsymbol{H}^{\mathrm{T}}_{\mathrm{bf}j}\boldsymbol{A}_{\mathrm{f}j\mathrm{b}} & \boldsymbol{M}_{\mathrm{f}j} \end{bmatrix},
$$

$$\boldsymbol{C}=\sum_{i=1}^{N}c_i\begin{bmatrix}\boldsymbol{J}_i\\ \boldsymbol{p}_i^{\times}\boldsymbol{J}_i\\ -\boldsymbol{J}_i\\ -(\boldsymbol{q}_i+\boldsymbol{r}_{\mathrm{db}})^{\times}\boldsymbol{J}_i\\ \dfrac{1}{c_i}\boldsymbol{C}_{\mathrm{f}}\end{bmatrix},$$

$$\boldsymbol{K}=\sum_{i=1}^{N}k_i\begin{bmatrix}\boldsymbol{J}_i\\ \boldsymbol{p}_i^{\times}\boldsymbol{J}_i\\ -\boldsymbol{J}_i\\ -(\boldsymbol{q}_i+\boldsymbol{r}_{\mathrm{db}})^{\times}\boldsymbol{J}_i\\ \dfrac{1}{k_i}\boldsymbol{K}_{\mathrm{f}}\end{bmatrix},$$

$$\boldsymbol{C}_{\mathrm{f}}=\begin{bmatrix}\boldsymbol{0}_{m\times 18} & \boldsymbol{C}_{\mathrm{f}1} & \boldsymbol{0}_m & \boldsymbol{0}_m\\ \boldsymbol{0}_{m\times 18} & \boldsymbol{0}_m & \boldsymbol{C}_{\mathrm{f}2} & \boldsymbol{0}_m\\ \boldsymbol{0}_{m\times 18} & \boldsymbol{0}_m & \boldsymbol{0}_m & \boldsymbol{C}_{\mathrm{f}3}\end{bmatrix},$$

$$\boldsymbol{K}_{\mathrm{f}}=\begin{bmatrix}\boldsymbol{0}_{m\times 18} & \boldsymbol{K}_{\mathrm{f}1} & \boldsymbol{0}_m & \boldsymbol{0}_m\\ \boldsymbol{0}_{m\times 18} & \boldsymbol{0}_m & \boldsymbol{K}_{\mathrm{f}2} & \boldsymbol{0}_m\\ \boldsymbol{0}_{m\times 18} & \boldsymbol{0}_m & \boldsymbol{0}_m & \boldsymbol{K}_{\mathrm{f}3}\end{bmatrix},$$

$$\boldsymbol{U}=\begin{bmatrix}\boldsymbol{E}_6\\ \boldsymbol{0}_{(3m+6)\times 6}\end{bmatrix}\begin{bmatrix}\boldsymbol{F}_{\mathrm{d}}\\ \boldsymbol{T}_{\mathrm{d}}\end{bmatrix}.$$

The force and torque propagating into the satellite can be rewritten as

$$\boldsymbol{F}_{\mathrm{e}}=\boldsymbol{C}_{\mathrm{e}}\dot{\boldsymbol{x}}+\boldsymbol{K}_{\mathrm{e}}\boldsymbol{x}, \tag{12}$$

where,

$$\boldsymbol{C}_{\mathrm{e}}=\sum_{i=1}^{N}c_i\begin{bmatrix}\boldsymbol{J}_i\\ (\boldsymbol{q}_i+\boldsymbol{r}_{\mathrm{db}})^{\times}\boldsymbol{J}_i\end{bmatrix},\quad \boldsymbol{K}_{\mathrm{e}}=\sum_{i=1}^{N}k_i\begin{bmatrix}\boldsymbol{J}_i\\ (\boldsymbol{q}_i+\boldsymbol{r}_{\mathrm{db}})^{\times}\boldsymbol{J}_i\end{bmatrix}.$$

Denoting $\boldsymbol{X}=[\,\boldsymbol{x}^{\mathrm{T}}\ \dot{\boldsymbol{x}}^{\mathrm{T}}\,]^{\mathrm{T}}$, Eqs. (11) and (12) can be described by the state equation as

$$\begin{aligned}\dot{\boldsymbol{X}}&=\boldsymbol{A}\boldsymbol{X}+\boldsymbol{B}\boldsymbol{u},\\ \boldsymbol{Y}&=\boldsymbol{C}_z\boldsymbol{X}+\boldsymbol{D}\boldsymbol{u},\end{aligned} \tag{13}$$

where

$$\boldsymbol{Y}=\boldsymbol{F}_{\mathrm{e}},\quad \boldsymbol{C}_z=\begin{bmatrix}\boldsymbol{K}_{\mathrm{e}} & \boldsymbol{C}_{\mathrm{e}}\end{bmatrix},\quad \boldsymbol{D}=\boldsymbol{0}_6,\quad \boldsymbol{u}=\begin{bmatrix}\boldsymbol{F}_{\mathrm{d}}\\ \boldsymbol{T}_{\mathrm{d}}\end{bmatrix},$$

$$\boldsymbol{A}=\begin{bmatrix}\boldsymbol{0}_{3m+12} & \boldsymbol{E}_{3m+12}\\ -\boldsymbol{M}^{-1}\boldsymbol{K} & -\boldsymbol{M}^{-1}\boldsymbol{C}\end{bmatrix},\quad \boldsymbol{B}=\begin{bmatrix}\boldsymbol{0}_{(3m+12)\times 6}\\ \boldsymbol{M}^{-1}\boldsymbol{E}_6\\ \boldsymbol{0}_{(3m+6)\times 6}\end{bmatrix},$$

So, the transmissibility matrix of the VIP with the two-parameter isolators can be obtained by Eq. (14) as follows

$$\boldsymbol{G}(s)=\boldsymbol{C}_z(s\boldsymbol{E}-\boldsymbol{A})^{-1}\boldsymbol{B}+\boldsymbol{D}. \tag{14}$$

3.2 Influence of the flexible solar arrays

The VIP for CMGs can not only isolate disturbances, but also transmit the effective torques to the satellite to execute attitude control. So when the VIP is used, the effective torque, which is below 2 Hz and caused by CMGs to satellite for completing attitude control, must not be influenced. As the rotor speed of the CMG is usually 6 000 rpm, the disturbances caused by the CMGs must be attenuated by more than 90% at frequencies above 100 Hz.

The parameters of the VIP are as follows

$$\boldsymbol{p}=\begin{bmatrix}0.5 & -0.25 & -0.25 & 0.5 & -0.25 & -0.25\\ 0 & 0.25\sqrt{3} & -0.25\sqrt{3} & 0 & -0.25\sqrt{3} & 0.25\sqrt{3}\\ 0 & 0 & 0 & 0 & 0 & 0\end{bmatrix},$$

$$\boldsymbol{q}=\begin{bmatrix}0.25 & -0.5 & 0.25 & 0.25 & -0.5 & 0.25\\ 0.25\sqrt{3} & 0 & -0.25\sqrt{3} & -0.25\sqrt{3} & 0 & 0.25\sqrt{3}\\ 0 & 0 & 0 & 0 & 0 & 0\end{bmatrix},$$

$$\boldsymbol{k}=\begin{bmatrix}-\sqrt{3}/2 & 0 & \sqrt{3}/2 & \sqrt{3}/2 & 0 & -\sqrt{3}/2\\ 0.5 & -1 & 0.5 & 0.5 & -1 & 0.5\\ 0 & 0 & 0 & 0 & 0 & 0\end{bmatrix},$$

where, $\boldsymbol{p}$ and $\boldsymbol{q}$ are the matrixes of the upper and the base platform points respectively. Because the VIP has 6 struts, $\boldsymbol{p}$ contains the six vectors $(\boldsymbol{p}_1,\boldsymbol{p}_2,\cdots,\boldsymbol{p}_6)$ and $\boldsymbol{q}$ also includes six vectors $(\boldsymbol{q}_1,\boldsymbol{q}_2,\cdots,\boldsymbol{q}_6)$. The unit of each vector is meter. $\boldsymbol{k}$ is the unit vectors along fixed axes of universal joints.

For the satellite system, $m_{\mathrm{p}}=82.8$ kg (the mass of each CMG is 19 kg), $m_{\mathrm{b}}=1\,120.75$ kg (the mass of each solar array is 40.25 kg), $\boldsymbol{I}_{\mathrm{p}}=\mathrm{diag}([\,9.47\ \ 9.47\ \ 18.72\,])$ kg·m^2,

$$\boldsymbol{I}_{\mathrm{b}}=\begin{bmatrix}1\,364 & -20 & -10\\ -20 & 1\,164 & -15\\ -10 & -15 & 1\,255\end{bmatrix}\mathrm{kg\cdot m^2}.$$

The three flexible solar arrays are the same, with the size of 2.3 m × 1.0 m. Their installation parameters are as follows

$$\boldsymbol{r}_{\mathrm{bf}1}=\begin{bmatrix}0 & r\cos 30^\circ & -0.55\end{bmatrix},$$

$$\boldsymbol{r}_{\mathrm{bf}2}=\begin{bmatrix}-r\cos^2 30^\circ & -r\cos 30^\circ\sin 30^\circ & -0.55\end{bmatrix},$$

$$\boldsymbol{r}_{\mathrm{bf}3}=\begin{bmatrix}r\cos^2 30^\circ & -r\cos 30^\circ\sin 30^\circ & -0.55\end{bmatrix},$$

where, $\boldsymbol{r}_{\mathrm{bf}j}$ is the vector from the centre of satellite body frame to the centre of the j-th flexible solar array frame, $r = 0.75$ m is the radius of the satellite bus, and j is the number of the solar arrays, $j = 1, 2, 3$.

The transformation matrix from the satellite body frame to the j-th flexible solar array frame is as follows

$$\boldsymbol{A}_{\mathrm{f1b}} = \boldsymbol{I}_{3\times3},\ \boldsymbol{A}_{\mathrm{f2b}} = \begin{bmatrix} \cos 120^\circ & \sin 120^\circ & 0 \\ -\sin 120^\circ & \cos 120^\circ & 0 \\ 0 & 0 & 1 \end{bmatrix},$$

$$\boldsymbol{A}_{\mathrm{f3b}} = \begin{bmatrix} \cos 240^\circ & \sin 240^\circ & 0 \\ -\sin 240^\circ & \cos 240^\circ & 0 \\ 0 & 0 & 1 \end{bmatrix}.$$

The vibration isolator element of the VIP can be simplified as a two-parameter model. In order to achieve satisfactory stability of the closed-loop system, the stiffness coefficient k and the damping coefficient c are selected as 150 000 N/m and 800 N·s/m, respectively, when the satellite has no flexible solar arrays. It is obtained that the corner frequencies of the VIP are in the range of 6.83 to 11.5 Hz and the corner frequency in the z-rotation direction (θ_z-direction) is 11.5 Hz which is higher than that in other direction. So it is crucial to analyze the influence of the flexible solar arrays on the performance of the VIP in the θ_z-direction.

According to Eq. (14), the vibration isolation system performance is predicted for different types of flexible solar arrays. Because the most important structure parameters of flexible solar array are modal frequencies and damping, so that firstly in this paper, the fundamental frequencies of these solar arrays are selected as 0.005 Hz, 0.05 Hz, 0.5 Hz and 1 Hz, respectively. The frequency response curves in the θ_z-direction can thus be drawn, and comparison of the performances of the VIP would be made below.

From Fig. 4, we can conclude that the transmissibility curve has some resonance peaks caused by the flexible solar arrays. When the resonance frequencies caused by flexible solar arrays are below the corner frequencies of the VIP, the effective torques to the satellite for the purpose of executing attitude control might be affected. Especially when the fundamental frequency of solar arrays is below 0.05 Hz, the effective torque is severely influenced. In Fig. 4, it is also

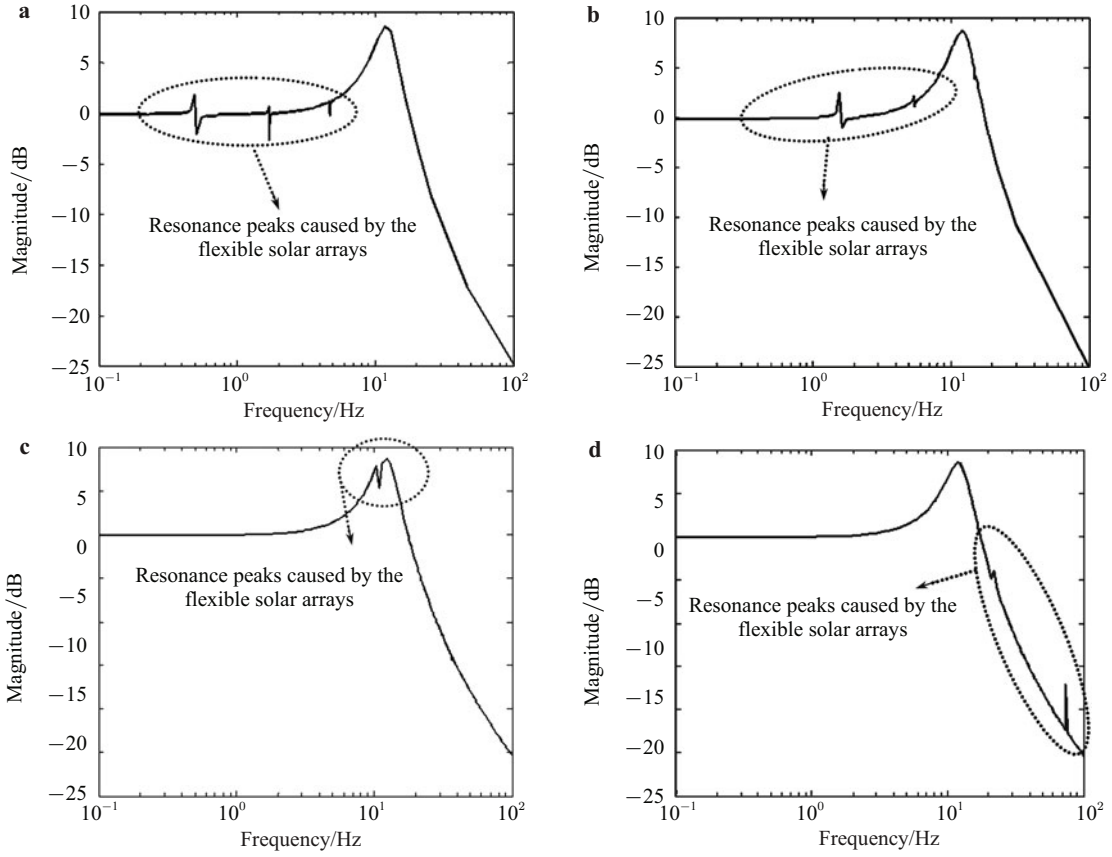

Fig. 4 Transmissibility curves for various fundamental frequency in the θ_z-direction: **a** 0.005 Hz; **b** 0.05 Hz; **c** 0.5 Hz; **d** 1 Hz

indicated that the influence of solar arrays on effective torques is small, when the fundamental frequency of solar array is high. Thus, the corner frequencies of the VIP should be selected below the resonance frequencies caused by flexible solar arrays so that the effective torques are guaranteed to be unaffected.

When the fundamental frequency of solar array is determined as 1 Hz, we can select different damping for it, and then draw different frequency response curves accordingly, as shown in Fig. 5. From Fig. 5, it is concluded that when the damping of solar array increased, the resonance amplification caused by the flexible solar array can be decreased.

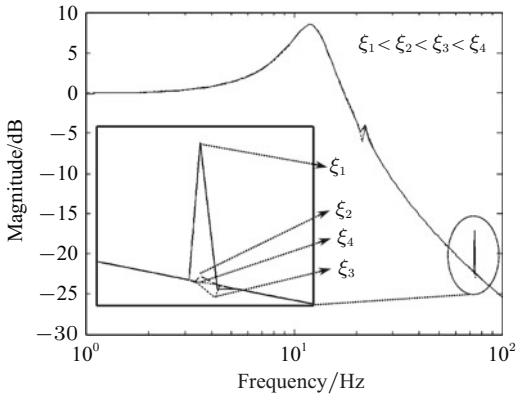

Fig. 5 Transmissibility curves for various damping coefficients in the θ_z-direction

In this research, a proportional integrate derivative (PID) controller is used to achieve the three-axis stability, and its parameters are chosen as $K_p = 2\,000$, $K_i = 0.1$, $K_d = 3\,200$ [31]. The bandwidth of attitude control system in each rotation direction is about 0.5 Hz. The parameters of the VIP are the same as above. The fundamental frequency of the solar array is selected as 1 Hz or so, and the first 3 order modal frequencies of the flexible solar array are as follows

$$\boldsymbol{\Lambda}_{f1b} = \boldsymbol{\Lambda}_{f2b} = \boldsymbol{\Lambda}_{f3b} = \begin{bmatrix} 1.02 & & \\ & 4.86 & \\ & & 6.35 \end{bmatrix} \text{Hz}. \tag{15}$$

Then various damping coefficients of the flexible solar array are selected. Figure 6 can be drawn accordingly, which shows the relationship between the system amplitude margin and the damping coefficient of the flexible solar array in the θ_z-direction. From Fig. 4, we can know that when the damping coefficient of the flexible solar array is smaller than 0.1%, the system is unstable. When the damping coefficient is larger than 0.15%, satisfactory stability can be achieved for the closed-loop system. So, the damping of solar array can not only make the resonance amplification caused by solar arrays decrease, but also improve the stability of the closed-loop system. The application of a damper device which is an integral part of the two flexible solar arrays in HST can convincingly demonstrate the reasonableness of the above conclusions [25].

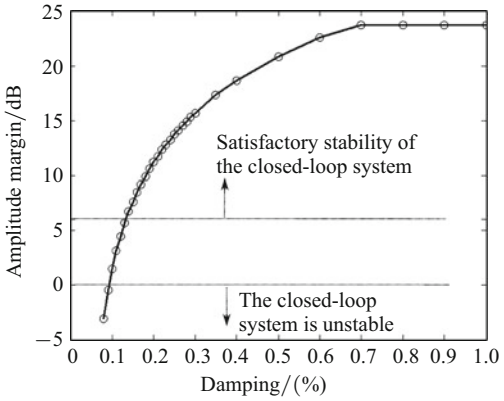

Fig. 6 Relationship between the system amplitude margin and the damping coefficient of the flexible solar array in the θ_z-direction

4 Simulations of the integrated satellite

According to the integrated satellite dynamic model for satellites furnished with flexible solar arrays, VIP and pyramid configured CMGs, the attitude angular velocities of the integrated satellite with and without the VIP have been simulated. In the present paper, the three initial attitude angles are all chosen as 1.5°. To avoid possible singularity, a robust pseudo inverse steering law is used [32]. The rotor motor, gimbal motor, attitude measurement and the external disturbing torque acting on the satellite are ignored in the present paper. In order to not affect the effective torques provided by CMGs and to make the attitude closed-loop system satisfactorily stable, the fundamental frequency of solar array is selected as 1 Hz with the first 3 order modal frequencies of the flexible solar array given in Eq. (15). The damping coefficient of the flexible solar array is selected as 0.7%.

The amplitude margin, phase margin and bandwidth for each rotation direction are shown as follows by using the above frequency domain analysis.

From Table 1, it is concluded that the above parameters for both the VIP and flexible solar arrays can satisfactorily meet the requirement of the system stability. Then the attitude angular velocities of the integrated satellite with and without the VIP are simulated by time domain method.

Table 1 Stability margins and bandwidth for each rotation direction

Direction	Amplitude margin/dB	Phase margin/(°)	Bandwidth/Hz
x-rotation	16.3	72.6	0.480
y-rotation	14.5	74.0	0.540
z-rotation	23.7	73.6	0.525

The simulation results of the attitude angular velocities are presented in Figs. 7 and 8, which shows that the attitude angular velocities can converge well to their equilibriums, and the response time is appropriate. It is further proved that the satellite can achieve attitude stabilization and the chosen parameters of the VIP and flexible solar arrays are reasonable. In Fig. 7, it is evident that the magnitude of the attitude stability is 6.2×10^{-6} rad/s under the disturbances caused by CMGs and flexible solar arrays. In Fig. 8, it is evident that the magnitude of the attitude stability is 3.8×10^{-7} rad/s with the VIP. Comparing Fig. 7 with Fig. 8, it is evident that the VIP is able to reduce the vibration amplitude of the attitude angular velocities to 6.1% of that under the disturbance of CMGs. Therefore, the VIP can attenuate the disturbance to a certain extent and can improve the attitude stability.

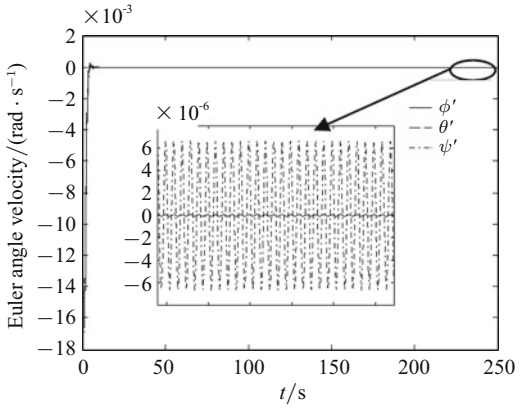

Fig. 7 Attitude angular velocities of the satellite without the VIP

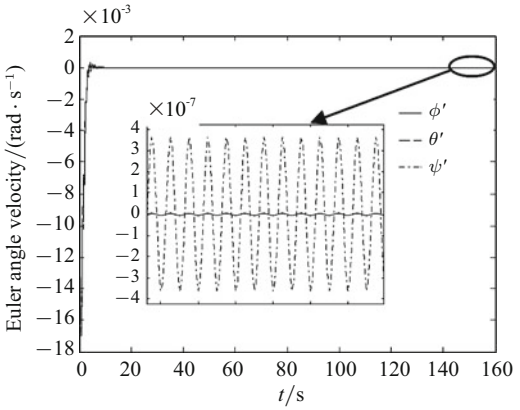

Fig. 8 Attitude angular velocities of the satellite with the VIP

5 Conclusions

In this paper, a passive multi-strut VIP was discussed for CMGs on satellites furnished with flexible solar arrays. A dynamic model was built for the integrated satellite with three flexible solar arrays, vibration isolation platform and CMGs, and the transmissibility matrix of the VIP was derived based on reasonable assumptions. The influences of flexible solar arrays on both the performance of the VIP and the stability of attitude control system are analyzed in detail. It is obtained that when the solar array has high stiffness, the influence of solar arrays on the effective torques is small. The damping of solar array can not only make the resonance amplification decrease, but also improve the stability of the closed-loop system. Selected parameters were used for both the VIP and flexible solar arrays to simulate the attitude stabilization, and their validity was tested by simulation results. The simulation results showed that the application of the VIP for CMGs could improve the attitude stability of the satellite to 0.078 rad/s.

On a satellite with a VIP of CMGs, the flexible solar arrays should be constructed as "stiff" as feasible in design. This would yield model frequencies as high as possible, which means less effect on the effective torques. A discrete damping device for solar arrays should be adopted to attenuate the disturbance caused by solar array and to improve the stability of the closed-loop control system.

References

1 Lei, J., Xu, S. J.: Underactuated spacecraft angular velocity stabilization and three-axis attitude stabilization using two single gimbal control moment gyros. Acta Mechanica Sinica **26**, 279–288 (2010)

2 Zhang, J. R., Rachid, A., Zhang, Y.: Attitude control for part actuator failure of agile small satellite. Acta Mechanica Sinica **24**, 463–468 (2008)

3 Li, J. F., Meng, X., Gao, Y. F., et al.: Study on relative orbital configuration in satellite formation flying. Acta Mechanica Sinica **21**, 87–94 (2005)

4 Davis, L. P., Hyde, T. T.: Moment control unit for spacecraft attitude control. United States Patent, 6340137, 2002-01-22

5 Kim, J., Agrawal, B.: Acquisition, tracking, and pointing technology development for bifocal relay mirror spacecraft. In: Proceedings of Beam Control Conference, Directed Energy Professional Society, Monterey, USA, March 21–24 (2006)

6 Peck, M. A., Cavender, A. R.: An airbearing-based tested for momentum-control systems. Advances in the Astronautical Science **114**, 427–446 (2003)

7 Baudoin, A., Boussarie, E., Damilano, P., et al.: A multi mission and multi cooperative program. In: Proceeding of the 52nd International Astronautical Congress, Toulouse, France, Oct. 1–5 (2001)

8 Anderson, E., Trubert, M., Fanson, J., et al.: Testing and application of a viscous passive damper for use in precision truss structures. In: Proceeding of the 32nd AIAA/ ASME/ ASCE/AHS/ASC Structures, Structural Dynamics, and Materials Conference, Baltimore, USA, Apr. 8–10, 2796–2808 (1991)

9 Davis, L. P., Workman, B. J.: Design of a D-Strut^{TM} and its application results in the JPL, MIT, and LaRC test beds. In: Proceeding of the 33rd AIAA/ASME/ASCE/AHS/ASC Structures, Structural Dynamics, and Materials Conference, Dallas, USA, Apr. 13–15, 1524–1530 (1992)

10 Davis, L. P., Cunningham, D., Harrell, J.: Advanced 1.5 Hz passive viscous isolation System. In: Proceeding of the 35th AIAA/ASME/ASCE/AHS/ASC Structures, Structural Dynam-

ics, and Materials Conference, Hilton Head, USA, Apr. 18–20 (1994)
11 Davis, L. P., Cunningham, D., Bicos, A., et al.: Adaptable passive viscous damper (an adaptable D-Strut^{TM}). In: Proceedings of the Conference, Smart structures and materials 1994: Passive damping, Orlando, USA, Feb. 14–16, 47–58 (1994)
12 Davis, L. P., Carter, D. R., Hyde, T. T.: Second generation hybrid D-strut. In: Proceedings of the Conference, Smart Structures and Materials 1995: Passive Damping, San Diego, USA, Mar. 1–2, 161–175 (1995)
13 Wilson, G. W., Wolke, P. J.: Performance prediction of D-Strut isolation systems. In: Proceeding of Passive Damping and Isolation Conference, San Diego, USA, Mar. 3–4 (1997)
14 Davis, L. P., Wilson, J. F.: Hubble Space Telescope reaction wheel assembly vibration isolation system. Structural Dynamics and Control Interaction of Flexible Structures, NASA Repot. N87-22702, 669–690 (1986)
15 Pendergast, K. J., Schauwecker, C. J.: Use of a passive reaction wheel jitter isolation system to meet the advanced X-ray astrophysics facility imaging performance requirements. In: Proceeding of Astronomical Telescope and Instrumentation Conference, Kona, USA, Mar. 20–28 (1998)
16 Bronowicki, A. J.: Vibration isolator for large space telescopes. Journal of Spacecraft and Rocket **43**, 45–53 (2006)
17 Basdogan, I., Grogan, R., Kissil, A., et al.: Preliminary optical performance analysis of the space interferometer mission using an integrated modeling methodology. Control of Vibration and Noise-New Millennium. In: Proceeding of International Mechanical Engineering Congress & Exposition 6th Biennial Symposium on Active Control of Vibration and Noise, Orlando, USA, Nov. 5-10 (2000)
18 Dewell, L., Pedreiro, N., Blaurock, C., et al.: Precision telescope pointing and spacecraft vibration isolation for the Terrestrial Planet Finder Coronagraph. In: Proceeding of UV/Optical/IR Space Telescopes: Innovative Technologies and Concepts II, San Diego, USA, July 31, 589902 (2005)
19 LoBosco, D. M., Blaurock, C., Chung, S. J., et al.: Integrated modeling of optical performance for the Terrestrial Planet Finder structurally connected interferometer. In: Proceeding of SPIE Modeling and Systems Engineering for Astronomy, 278–289 (2004)
20 Miller, S. E., Kirchman, P., Sudey, J.: Reaction wheel operational impacts on the GOES-N jitter environment. In: Proceeding of AIAA Guidance, Navigation and Control Conference and Exhibit. Hilton Head, USA, Aug. 20–23 (2007)
21 Liu, K. C., Maghami, P.: Reaction wheel disturbance modeling, jitter analysis, and validation tests for Solar Dynamics Observatory. In: Proceeding of AIAA Guidance, Navigation and Control Conference and Exhibit, Honolulu, USA, Aug. 18–21 (2008)
22 Gary, M., Mike, F., Kong, H., et al.: Fine pointing control for a next generation space telescope. Space telescopes and instruments V. In: Proceedings of the Conference, Kona, USA, Mar. 25–28, 1070–1077 (1998)
23 Luis, M., Frank, T., Satya, A., et al.: Line of sight stabilization for the James Webb Space Telescope. Advances in the Astronautical Sciences **121**, 17–30 (2005)
24 Zhang, Y., Xu, S. J.: Vibration isolation platform for control moment gyroscopes on satellites. Journal of Aerospace Engineering (2011) DOI: 10.1061/(ASCE)AS.1943-5525.0000156
25 Anandakrishnan, S. M., Connor, C. T., Lee, S., et al.: Hubble Space Telescope solar damper for improving control system stability. In: Proceeding of Aerospace Conference Proceedings, 2000 IEEE, USA, Mar. 18–25, 261–276 (2000)
26 Zeng, X. Y., Li, J. F., Baoyin, H. X., et al.: Trajectory optimization and applications using high performance solar sails. Theor. Appl. Mech. Lett. **1**, 033001 (2011)
27 Dasgupta, B., Mruthyunjaya, T. S.: A Newton-Euler formulation for the inverse dynamics of the Stewart platform manipulator. Mechanism and Machine Theory **33**, 1135–1152 (1998)
28 Mahboubkhah, M., Nategh, M. J., Khadem, S. E.: A comprehensive study on the free vibration of machine tools' hexapod table. The International Journal of Advanced Manufacturing Technology **40**, 1239–1251 (2009)
29 Zhang, Y., Xu, S. J.: High frequency vibration isolation of CMG for satellites. Journal of Astronautics **32**, 1722–1727 (2011)
30 Jin, L.: Study on attitude dynamics and control of spacecraft using angular momentum exchange devices. [Ph.D. Thesis], Beihang University, Beijing (2008)
31 Zhang, J. R., Xu, S. J., Li, J. F.: A new design approach of PD controllers. Aerospace Science and Technology **9**, 329–336 (2005)
32 Jin, J., Zhang, J. R., Liu, Z. Z.: Error analysis and a new steering law design for spacecrafts control system using SGCMG. Acta Mechanica Sinica **27**, 803–808 (2011)